Research on Biomedical Engineering (2024) 40:281–296
https://doi.org/10.1007/s42600-024-00342-x

REVIEW

Sol–gel-templated bioactive glass scaffold: a review

Maryam Sarmast Shoushtari[1] · David Hoey[2,3,4] · Dayang Radiah Awang Biak[1,5] · Norhafizah Abdullah[1] · Suryani Kamarudin[1] · Halimatun S. Zainuddin[1]

Received: 26 January 2023 / Accepted: 3 February 2024 / Published online: 23 February 2024

Abstract

Purpose This review paper explores diverse synthesis strategies within the sol–gel technique for producing silicate bioglass with a focus on tailoring these materials for bone scaffold design.

Method A comprehensive search was conducted across various databases, including ScienceDirect, Taylor & Francis, PubMed, Hindawi, Royal Society of Chemistry (RSC), Wiley Online Library, ResearchGate, and Google Scholar, using keywords such as "silica bioglass," "Sol–gel technique," "Templating," and "Bone scaffold." The analysis considered variables such as the sol–gel method, the templating approach, and materials used to fabricate silica bioglass bone scaffolds. Out of 140 initially identified studies, 92 were selected for detailed review published within the last two decades.

Result and conclusion In this study, the effect of the sol–gel fabrication technique on the improvement of the structure of silicate bioglass bone scaffolds has been reviewed, along with a consideration of the associated advantages and disadvantages. Specifically, the focus of this study was on the templating sol–gel method and its direct impact on morphology and pore structures. Consequently, these findings have evaluated the development of templating sol–gel fabrication techniques for enhancing the bioactivity and biocompatibility of bone scaffolds.

Keywords Silicate bioglass · Sol–gel · Templating · Bone scaffold

Abbreviations

BC	Bacterial cellulose
BG	Bioglass
CNF	Cellulose nanofiber
CTAT	Hexadecyltrimethylammonium P-toluenesulfonate
CTAB	Hexadecyltrimethylammonium bromide
HA	Hydroxycarbonate apatite
HMBG	Hollow mesoporous bioactive glass
hMSCs	Human marrow mesenchymal stem cells
hPDLCs	Human periodontal ligament cells
IGFs	Insulin-like growth factors
MBG	Mesoporous bioglass
PAA	Polyacrylic acid
PEG	Polyethylene glycol
PMAA	Polymethyl methacrylate
PVA	Polyvinyl alcohol
SBF	Simulated body fluid
TEOS	Tetraethyl orthosilicate
TMOS	Tetramethoxysilane
TEA	Triethanolamine

✉ David Hoey
dahoey@tcd.ie

✉ Dayang Radiah Awang Biak
dradiah@upm.edu.my

1 Department of Chemical & Environmental Engineering, Faculty of Engineering, Universiti Putra Malaysia, 43400 Serdang, Selangor, Malaysia

2 Trinity Centre for Biomedical Engineering, Trinity Biomedical Sciences Institute, Trinity College Dublin, Dublin, Ireland

3 Department of Mechanical, Manufacturing, and Biomedical Engineering, School of Engineering, Trinity College Dublin, Dublin, Ireland

4 Advanced Materials and Bioengineering Research Centre, Trinity College Dublin & RCSI, Dublin, Ireland

5 Institute of Nanoscience and Nanotechnology, Universiti Putra Malaysia, 43400 Serdang, Selangor, Malaysia

Introduction

Bioactive glasses are introduced as a particular subcategory of oxide-based biocompatible ceramics (Jones 2015). Hench introduced "bioglass" to the world and defined these materials as "… could elicit a controlled action and reaction in the

physiological environment" (Crovace et al. 2016). The main specification of bioglass, which differentiates them from other types of bioceramics, is a hydroxycarbonate apatite (HA) layer that is typically formed when the material is soaked in simulated body fluid (SBF). The ionic concentration of SBF is close to that of human blood plasma (Arcos & Vallet-Regí, 2010; Kokubo & Takadama 2006). Bioactive glasses have different families, and each family has its signature chemical composition. The main groups of bioactive glass include phosphate-based glasses, silicate-based glasses, and borate-based glasses (Jones 2015). Silicate bioglasses have always received much interest compared to two other types of bioactive glasses due to their more significant chemical and thermal stability, which enables simple synthesis and processing of these glasses as well as the ability to tailor their chemical compositions to achieve the desired properties (Baino 2021). Hence, silicate glasses have been the most favorable and fascinating biomaterials over the last 50 years (Deshmukh et al. 2020).

The properties of the final product (such as bioactivity, density, specific surface area, and pore-volume), quality, and cost are highly dependent on the processing techniques used (Deshmukh et al. 2020; Dziadek et al. 2017). Chemical stabilization, calcination, and processing conditions such as time and temperature significantly affect the formation of the crystalline phase of the bioglass. These processes also affect the formed crystals' microscopic structure and sintering behaviors (Mukundan et al. 2013). There are two main techniques to synthesize bioactive glass: melting and sol–gel techniques.

The melting technique is the conventional method for producing bioglass on a commercial scale (Faure et al. 2015; Jones 2015). In the melt-quenching process, oxides, carbonates, and phosphate compounds are mixed and melted in a platinum crucible at a temperature above 1300 °C. Then, the melted mixture is quenched to room temperature in a graphite mold to form rods or monoliths or in water to form frit. The solidified compound is then milled to obtain bioglass powder (Bellucci et al. 2017; Brauer 2015; Jones 2015; Kaur et al. 2014). The main disadvantage of this technique is the high synthesis temperature (1100–1450 °C) (Jones 2015; Owens et al. 2016). On the other hand, the longtime thermal process increases the grain size (Venkatraman & Swamiappan 2020). Furthermore, the melting method often leads to the formation of low-purity products due to chemically heterogeneous materials and some contaminants. This occurrence can be due to the processes, i.e., primary crystallization with precipitation or the presence of unreacted solid chemicals (Siqueira et al. 2011). Moreover, the final bioglass powder formed has limited porosity and low specific surface area (Siqueira et al. 2011; Zheng & Boccaccini 2017). In 1990, Li et al. introduced sol–gel as a novel bioglass processing technique (Li 1991). In this approach, a suspension of small colloidal is constructed and then interconnected to create a 3D network gel structure (Jones 2015; Kaur et al. 2016; Lei et al. 2020). One to 1000 nm in diameter solid particles or polysilanes were suspended in liquid (Lei et al. 2020). This mechanism converts phosphorous-containing alkoxides and calcium salt into bioglass via hydrolysis, polycondensation, ageing, drying, and thermal stabilization, sequentially (Albert et al. 2017; El-Rashidy et al. 2017; Owens et al. 2016). Peltola et al. described how glasses made via the sol–gel process have improved bioactivity (Peltola et al. 1999).

Typically, templating is used to grow tubular channels in materials in order to increase porosity and enhance the interstitial network (Sarmast Sh et al. 2022). The use of natural materials as a sacrificial template, such as wood cells and sugarcane, has been investigated in order to design and fabricate similar structures composed of wide and varied material components such as hydroxyapatite (Dong et al. 2002; Qian et al. 2009). To develop porous bone implants, this method has been used to replicate pre-existing natural forms, such as the tubular structures found in native pinewoods and rattan, in chemically engineered materials composed of hydroxyapatite. Generally, due to the ease with which complex and elaborate structures with high functional specificity can be found in nature, natural species templating has developed into a versatile approach for fabricating advanced materials with sophisticated structure and morphology (Zheng et al. 2015). Templated silica bioglass has distinct advantages that make it an intriguing research area (Albert et al. 2017). This paper reviews the recent studies on templating methods to assist the sol–gel one scaffold were covered. Figure 1 shows the illustration of screening process for studies included in the review from 1991 to 2023.

Method

Sol–gel technique

The following section introduces and discusses the synthesis strategies of the sol–gel technique to produce silicate bioglass.

Acid-/base-catalyzed synthesis

Bioglasses can be fabricated using an acid-catalyzed approach, where a rich inorganic acid acts as the catalyst. Nitric acid (HNO_3), sulfuric acid (H_2SO_4), and hydrochloric acid (HCl) are commonly used catalysts due to their rapid initiation of the hydrolysis reaction. In acidic conditions, H^+ ions, and in primary conditions, OH^- ions attack silicate precursors, leading to the formation of silanol groups during hydrolysis. The water/alcohol condensation process generates siloxane bridges (Si–O–Si) by cross-linking silanol/silanol or silanol/ethoxy groups. The hydrolysis process in

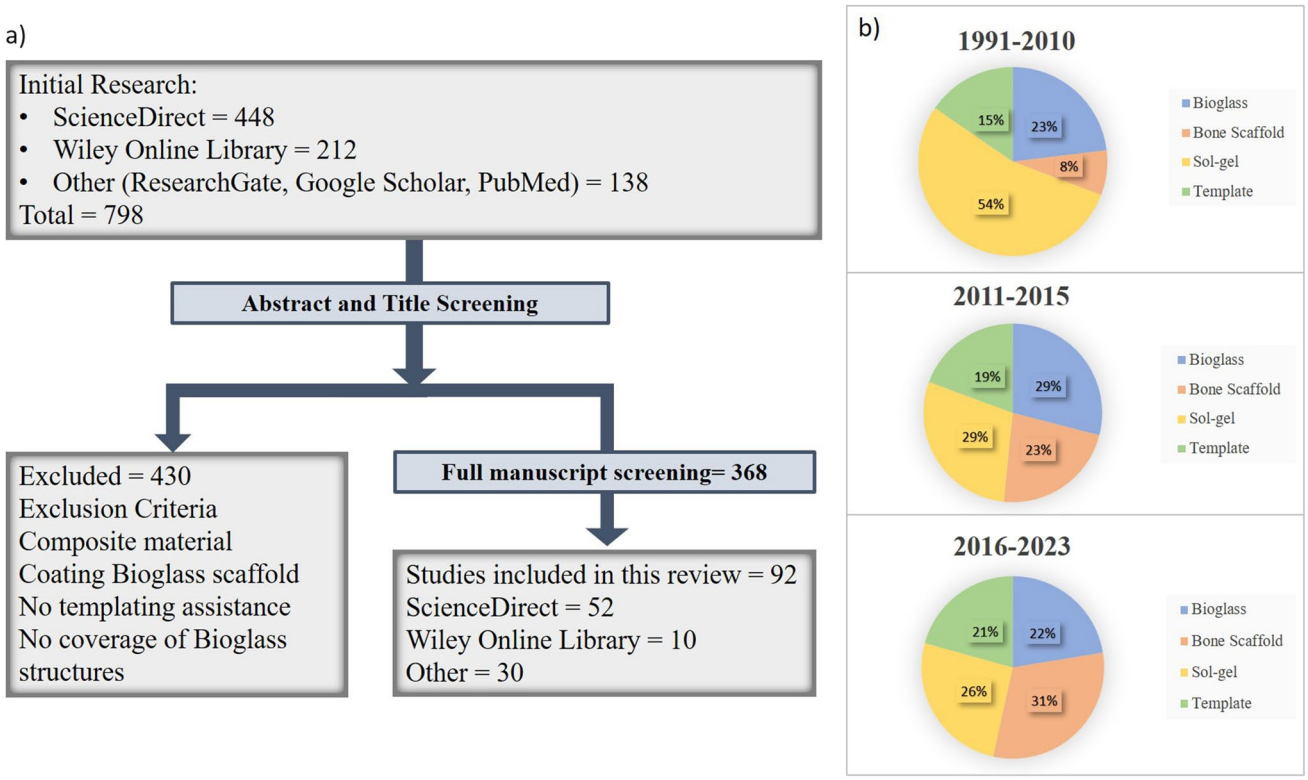

Fig. 1 **a** Paper selection process and publication distribution. **b** Publication related on the research from 1991 to 2023

acidic conditions determines the rate of hydrolysis, while the condensation process dictates the rate in primary states. The acid-catalyzed reaction produces small linear polymeric entities that enhance hydrolysis and end-of-chain condensation. However, during the gelation step, cross-linking these linear polymers results in a flimsy structure that crumbles upon drying (Albert et al. 2017; Brinker and Scherer 2013; Zheng & Boccaccini 2017).

On the other hand, base catalysis promotes cross-linking and the formation of ramified polymers, which can create smooth colloids when combined with significant dissolution. Using base catalysts can aid in particle formation by increasing the pH value, thus preventing the formation of bulky gel structures in bioglasses. In the sol–gel synthesis of silica bioglass based on acid/base catalysis, the process starts by adding TEOS to metal ion precursors under acidic conditions, followed by adding a concentrated primary catalyst to accelerate the reaction. While tiny colloidal particles can form 3D gel networks under acidic conditions, salt's presence reduces the nanoparticles' stability (Xia & Chang 2007). Consequently, silicate glasses typically exhibit a polydisperse or agglomerated morphology. The pH of the sol directly affects the hydrolysis process and indirectly impacts the mechanical properties of the final product (Kaur et al. 2016). For instance, increasing the pH from 1.5 to 9 reduces shrinkage from 15 to 1.5% (Woignier et al. 1994). Another study indicates that raising the pH of the sol results in larger silica gel particles with stiffer silica branches (Wen et al. 2018).

Microemulsion-based synthesis

Microemulsions, which are isotropic, homogeneous, and thermodynamically stable liquid mixtures, differ from conventional emulsions as they can be formed simply by mixing components and utilizing surfactants as stabilizers (Deshmukh et al. 2020; Zheng & Boccaccini 2017). These microemulsions fall into three categories: oil dispersed in water (direct), water dispersed in oil (reverse), and bicontinuous microemulsions. Reverse microemulsions, for instance, are predominantly used in the production of silica bioactive glass (Zheng & Boccaccini 2017). The oil phase comprises long-chain hydrocarbons, while the surfactants consist of long-chain organic molecules with a hydrophilic head and a lipophilic tail (Deshmukh et al. 2020). In addition to catalysts, the aqueous phase contains silicate and metal ion precursors. The silicate precursors undergo hydrolysis and condensation in water droplets that act as reactors.

Silicate and metal ion precursors are present in the aqueous phase, along with catalysts. The silicate precursors undergo hydrolysis and condensation within water droplets, which function as reactors. However, the water droplets

often collide through Brownian motion and coalesce into larger droplets. This collision and coalescence can be detrimental to achieving a homogeneous glass composition. To counteract this, the surfactants play a crucial role in stabilizing the microemulsion droplets, preventing the aggregation of nanoparticles. Consequently, the synthesized glass exhibits a homogenous composition and dispersion with varying particle sizes due to the breakage of microemulsion drops during collisions. Before drying and calcination, vigorous washing is necessary to remove excess surfactants and the oil phase to avoid the formation of organic residues and nanoparticle aggregations (Zheng & Boccaccini 2017). Moreover, the size of the particles can be adjusted by fine-tuning the microemulsion droplets. For example, altering catalyst concentrations can lead to size variations (Wang & Chen 2017). Liang et al. (Liang et al. 2015) discovered that bioglass could be obtained in spherical shape by adjusting the aqueous ammonia concentration. The size and shape of bioglass nanoparticles are significantly influenced by the concentration of aqueous ammonia during the synthesis process. Low ammonia concentrations (1 mol L^{-1}) yield nanospheres with a surface area and small average pore diameter. Intermediate ammonia concentrations (3 mol L^{-1}) form radial nanospheres, which exhibit a lower surface area but larger average pore diameter. High ammonia concentrations (5 mol L^{-1}) also produce radial nanospheres with the largest average pore diameter among the samples. The results are summarized in Table 1.

Modified sol–gel synthesis

In this section, various studies that have explored modified sol–gel synthesis methods to control the microstructure of silicate glasses will be discussed.

Ethanol washing as an alternative

Mukundan et al. (Mukundan et al. 2013) proposed using ethanol washing as an alternative to the conventional heat treatment calcination to stabilize bioactive glass. According to their findings, ethanol washing resulted in higher pore volume, diameter, and specific surface area compared to the heat treatment process. A summary of their characterization findings can be found in Table 2.

Table 2 Characterization of bioglass with ethanol wash (BG-E) and without ethanol wash (BG) effect (Mukundan et al. 2013)

Characterization	*BG*	*BG-E*
Particle size (μ)	5.88 ± 1.35	0.63 ± 0.22
True density (g/cm^3)	3. 21	3.22
Bulk density (g/cm^3)	0.270 ± 0.006	0.170 ± 0.002
Total porosity (%)	91.5	94.7
Specific surface area (m^2/g)	94	290
Average pore diameter (A^0)	57	100
Total pore volume (cm^3/g)	0.0006	0.012

Influence of citric acid

The role of citric acid in the hydrolysis reaction and gel transformation to achieve high structural homogeneity on bioglass 58S was investigated by Lopes et al. (Lopes et al. 2019). According to the findings, citric acid molecules act as an adequate molecular template formed by intermolecular forces. Hydrogen bonds are formed by chemical interactions between the hydroxyl groups and COOH. Citric acid controls the segregation phase of the gel during the drying and heat transfer steps by creating chemical interactions between hydrogen bonds and the superficial silanol groups on the small-sized silica nanoparticles in the sol, thus regulating their growth to the backbone of the gel. Moreover, the self-propagating heating behavior of the nitrate-citrate in the xerogel during the thermal step permitted the removal of the organic load and stabilization of the vitreous structure at a temperature significantly lower than the conventional sol–gel method. Furthermore, the enthalpy involved in the conventional 58S crystallization process is less than that observed for the modified 58S. ΔH_c for conventional 58S was − 184 mJ mg^{-1}, and the modified one was − 210 mJ mg^{-1}.

Colloidal and polymeric techniques

Spirandeli et al. (Spirandeli et al. 2020) used colloidal and polymeric techniques to create bioglass 45S5 using two different silica precursors. Tetraethyl orthosilicate metal alkoxide ($Si(OC_2H_5)_4$ – TEOS) is used in the polymeric approach, while silicic acid is used in the colloidal process (H_4SiO_4). The results showed similar bioglass

Table 1 Effect of aqueous ammonia concentration on bioglass nanoparticle morphology and porous properties (Liang et al. 2015)

Aqueous ammonia concentration (mol L^{-1})	*Morphology*	*Specific surface area (m^2/g)*	*Average pore diameter (nm)*	*Total pore volume (cm^3/g)*
1	Nanospheres	418.01	7.01	0.546
3	Radial nanospheres	315.07	9.17	0.708
5	Radial nanospheres	225.38	12.59	0.698

functional groups, crystalline phases, and morphology in both groups. However, replacing TEOS with silicic acid as a precursor reduced the total synthesis time from 13 to 1 day. Furthermore, the number of NBO bonds and bioactive phases formed after calcination in colloidal BG was significantly higher than in polymeric BG. Hence, the colloidal BG performed better in vitro bioactivity concerning HA layer formation and dissolution capacity in the SBF solution.

Fast-drying method

Ben-Arfa et al. (Ben-Arfa et al. 2018) synthesized 67Si–24Ca–10Na–8P using two different drying methods: conventional and fast-drying. First, a rotary evaporator was used to dry the sol in the fast-drying method under 50 mbar at 550 °C for 1 h. This drying process was around 300 times faster than the traditional method. Next, both samples were thermally stabilized for an hour at 550 °C. The result revealed very similar silica network structures in both groups. However, the fast-dried bioglass showed a slightly lower degree of polymerization. In addition, the fast-dried bioglass showed more remarkable growth of crystalline HA, especially during the initial immerging period with SBF. Another study by these authors (Ben-Arfa et al. 2020), synthesized 67Si–24Ca–10Na–8P using two different precursors and catalysts with the fast-dried technique. The first group used acetate salt precursors and nitric acid (BGA), whereas the second group used nitrate salts and citric acid (BGN) as precursors and catalysts. Despite being primarily amorphous, BGA contains small amounts of crystalline phases such as HA and silica (coesite). The higher pH environment may assist the formation of these phases and faster condensation reactions, resulting in lower levels of network polymerization, closed porosity, prior particle, lower specific surface area, and agglomeration. These characteristics favored the exhibition of the undesired calcite ($CaCO_3$) phase in vitro. However, the condensation rate reduced BGN syntheses from nitrate precursors in lower pH settings. The amorphous glass structures with more significant polymerization levels, specific surface area, and density tend to have the highest in vitro bio-mineralization rates. Due to the high amounts of nitric acid used as a catalyst and its interaction with acetate species, poor extraction of nitrate byproducts was observed in the BGA group. Using alternative metal salt precursors, such as nitrate and acetate, made a reasonable adjustment in the network connectivity and specific surface area of both glasses, which play an essential role in modifying the bioactivity of the sol–gel bioglasses (Ben-Arfa et al. 2020).

Freeze-casting method

Fantecle et al. (Fantecelle et al. 2023) used freeze-cast scaffolds to fabricate a bioactive glass derived from the SiO_2–CaO–Na_2O–P_2O_5–K_2O–MgO system, with a sintering temperature set at 650 °C for a duration of 2 to 8 h. This specific temperature and time frame have been selected to promote viscous flow sintering while preventing crystallization. During the freeze-casting process, water is employed as a solvent, and liquid nitrogen serves as the coolant. The result of this study is displayed in Table 3.

Nitrate-free sol–gel process

The organic, nitrate-free sol–gel process, for example, uses lactic acid and citric acid to create high structural homogeneity bioglass within 45 days (Lopes et al. 2019). Electrospinning assisted by sol–gel is a common technique for producing MGB fibers. Using sol–gel derived, MGB has a homogeneous structure with controllable porosity and great cytocompatibility (Deepthi et al. 2016). The sol–gel MGB approaches macro-pore channels with foaming agents such as surfactants and hydrogen peroxide or porogen materials, including polyvinyl alcohol, polystyrene spheres, and polyethylene glycol (Owens et al. 2016).

Templated sol–gel scaffold

The templated sol–gel scaffold is a versatile method for controlling the morphology and structure of bioglass. This process involves foaming the sol with the aid of a surfactant and is followed by condensation and gelation reactions to achieve a porous scaffold. The use of templates plays a crucial role in controlling the pore architecture of the scaffold. For example, templating processes can create channels in particles and increase the porosity, leading to improved internal network growth. Surface properties of the scaffold are also important as they can affect the distribution of molecules and ions. The interactions between molecules/ions and the surface of the

Table 3 Characterization of bioglass with sintered from 2 to 8 h (Fantecelle et al. 2023)

Characterization	*2 h*	*4 h*	*8 h*
Total porosity (μ%)	63	67	65
Bulk density (g/cm^3)	0.99 ± 0.02	0.88 ± 0.02	0.92 ± 0.02
Young's modulus (GPa)	1.24 ± 0.01	1.40 ± 0.02	1.10 ± 0.01
Compressive strength (MPa)	22.4 ± 3.1	12.7 ± 0.8	20.4 ± 2.5
Toughness ($\times 10^{-2}$ J m^{-3})	26.9	4.9	27.0

material depend on its surface properties. This phenomenon allows for precise control over the structure of the material synthesized within the confinement space of a template on a sub-micrometer scale. The specific surface area and bioactivity of the material can be influenced by the amount of template added. Various templates have been used in the synthesis of bioglass scaffolds. Zeolitic wood cells (Dong et al. 2002), sugarcane (Qian et al. 2009), hexadecyltrimethylammonium bromide (CTAB) (Anand et al. 2018; Firuzeh et al. 2021; Letaïef et al. 2014; Wen et al. 2022; Xie et al. 2020), cellulose nanofiber (CNF) (Sarmast Sh et al. 2022), and bacterial cellulose (BC) (Luo et al. 2017a, b; Luo et al. 2017a, b; Wen et al. 2018; Xiao et al. 2019) have been utilized as templates to control the structure and properties of the bioglass scaffolds. Figure 2 shows a schematic of sol–gel with templating assistance. Table 4 summarizes pros and cons of each technique.

Result

Surfactant usage as template

To prepare a sol–gel bioglass scaffold, foaming the sol involves a surfactant's aid. This process is followed by condensation and gelation reactions to achieve a porous scaffold. However, this method has only been used for a few bioglasses, such as 58S and 70S30C (Fu et al. 2012; Owens et al. 2016). These three-dimensional scaffolds have a hierarchical pore architecture consisting of interconnected mesopores (2–50 nm) (Fu et al. 2012; Naleway et al. 2015). Moreover, the interactions of molecules and ions with the surface of a material are highly dependent on the surface properties of the material. As a result, the surface properties may affect the distribution of molecules or ions near

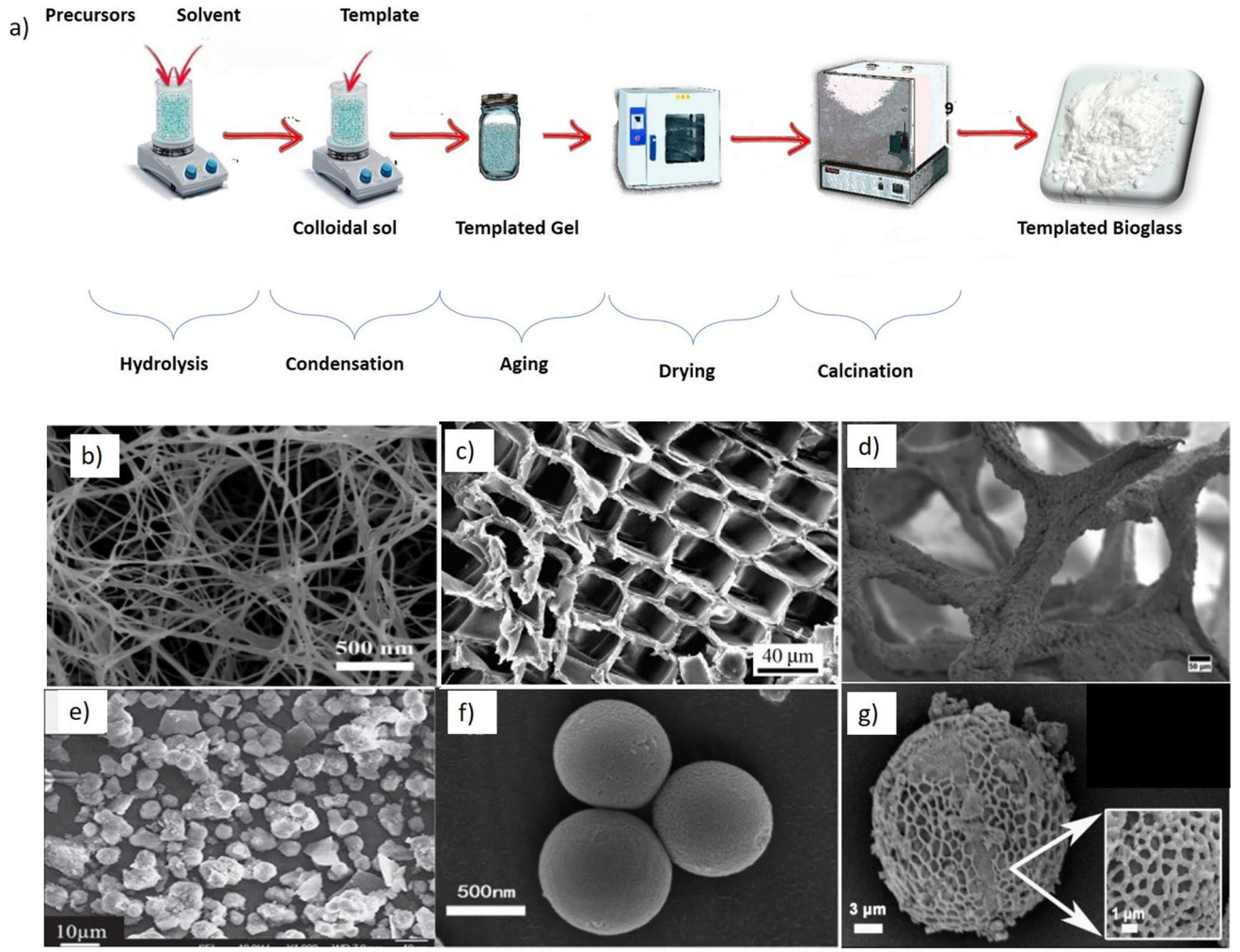

Fig. 2 **a** Schematic of sol–gel templating technique. **b** BG-BC template (Wan et al. 2009)*, **c** BG-sugarcane template (Qian et al. 2009)*, **d** BG-PVA template (Nawaz et al. 2023)*, **e** BG-chitosan template (Lei et al. 2012)**, **f** BG-CATAB template (Wang & Chen 2017)*, **g** BG-pollen template (Zheng et al. 2015)*. *Copyright by Elsevier, **Copyright by Willey

Table 4 Advantages and disadvantages of different sol–gel technique

Sol–gel technique	*Advantages*	*Disadvantages*	*References*
Acid-/base-catalyzed	Simplicity and versatility in controlling the reaction conditions, such as pH and temperature	Require longer curing times and higher temperatures to achieve complete gelation and densification. To reduce drying times, the xerogel method is suggested to produce the gel	(Bokov et al. 2021; Deshmukh et al. 2020; Lei et al. 2020; Zheng & Boccaccini 2017)
	The gel network formation at ambient conditions	It can lead to the formation of undesirable byproducts. By optimizing reaction conditions, such as the pH, the formation of undesirable byproducts can be minimized. For example, with the addition of alcohol, the solution becomes more dilute, and the reaction rate decreases sharply	
	Ability of the incorporation of various dopants or additives	Require careful handling of corrosive acids or bases	
Microemulsion-based	Excellent control over the particle size, morphology, and distribution	Complex preparation procedures. Adding co-surfactant resulting in an interphase pressure that exceeds the initial positive interfacial tension	(Deshmukh et al. 2020; Lei et al. 2020; MODAN & PLĂIAȘU, 2020; Zheng & Boccaccini 2017)
	Highly uniform and monodisperse particles formation	Requiring the specialized surfactants and organic solvents. For example, adding carbon chain 4–8 aliphatic alcohol used to have transparent sol	
	Ability to synthesis of hollow or mesoporous structures	Removing organic chemical may require additional steps or post-treatments	
Modified sol–gel	Creation of hierarchical pore architectures	The choice of modification technique can significantly influence the resulting structure and properties of the scaffold	(Ben-Arfa et al. 2018, 2020; Firuzeh et al. 2021; Lopes et al. 2019; Spirandeli et al. 2020)
	Precise control over the material's structure on a sub-micrometer scale		
Templated sol–gel	The addition of templates or sacrificial agents could control the structure and porosity of the bioglass scaffold	The choice of template material and concentration of the agents significantly influence the resulting structure and properties of the scaffold	(Albert et al. 2017; Deshmukh et al. 2020; Ji et al. 2019)
	It allows for the creation of hierarchical pore architectures and precise control over the material's structure on a sub-micrometer scale	Finding the optimal template conditions may require extensive experimentation	
		The removal of templates can also be challenging and may affect the final properties of the scaffold	

the material surface. This phenomenon can be significant enough to allow for precise control over the structure of a material synthesized within the confinement space of a template on a sub-micrometer scale (Guo et al. 2017). For example, to control the morphology of silica nano-bioglass, a template can be added to confine silica templating processes are generally used to create channels in particles and increase the porosity to improve the internal network growth.

On the other hand, templated sol–gel processing is a reliable method with minimal treatment and, most of the time, easily obtained (Albert et al. 2017; Zheng & Boccaccini 2017). However, it should be used within certain limits, as increasing the liquid base template concentration results in spherical, rod-shaped, and flexible bilayer structures and reversed micelles formation. The amount of template added directly relates to the appearance of mesoporous architecture and affects the specific surface area and bioactivity of MBG particles (Ge et al. 2019; Huang et al. 2013). It has been reported that using sol–gel and surfactant foaming methods combined with vigorous mechanical sintering (at 1000 °C for 2 h), the mechanical strength was significantly improved (Chen & Thouas 2011).

Influence of CATAB as templates on sol–gel process

Wang et al. described a simple technique to produce hollow mesoporous bioglass (HMBG) by combining the sol–gel with the microemulsion technique. Microemulsion droplets of hexadecyltrimethylammonium bromide (CTAB) were formed as a hollow cavity template by mixing cyclohexane, ethanol, and water. HMBG had a controllable shell thickness. By varying the CTAB concentration, the HMBGs with varying shell thicknesses and cavity sizes were synthesized. The results showed that CTAB was critical in modulating the HMBGs nanoparticles' interior mesoporous morphology, structure, and dispersion (Wang & Chen 2017). As the CTAB concentration was increased the shaping of the samples depicted a dynamic process from sphere to short rod then to long rod (Li et al. 2015). Moreover, the shape of the samples changed dynamically as the CTAB concentration was increased, from sphere to short rod to long rod (Hu et al. 2014).

Xie et al. (Xie et al. 2020) created a uniform, monodispersed radial MBG with a high calcium and phosphorus content. First, they synthesized the radial mesoporous SiO_2-$P2O_5$ nanosphere (SPN) in a cyclohexane-water biphasic stratification reaction system with triethanolamine (TEA) as a hydrolysis catalyst and CTAB as a template. Then, the SiO_2–CaO–P_2O_5 was synthesized using SPN as both the phosphorus, silicon, and calcium ($Ca(NO_3)_2$) sources in solid reactions. The MBG exhibited a radial structure with ~ 7 nm pore size, 0.85 $cm^3\ g^{-1}$ pore volume, and a high specific surface area (321 $m^2\ g^{-1}$). The EDS results showed that increasing the reaction temperature from 60 to 70 °C, the P_2O_5 content was also increased from 0.53 to 1.16 mol%. Finally, MBG was co-cultured with mMSCs. The result revealed no effect on cell viability at a concentration of 50 μg mL^{-1}, which was attributed to the network's high Ca^{2+} content, which would hasten the biodegradation of MBG after it was absorbed by cells.

In a recent study, Wen et al. (Wen et al. 2022) assessed the effect of nitrogen on the bioglass structure ($60SiO_2$–30.8CaO–$9.2P_2O_5$) by using CTAB as a template. During the sol–gel process, they used $C_2H_8N_2$ (the nitrogen source) and absorbed it into bioglass. It has been demonstrated that all samples have a uniform interstitial mesoporous nanosphere microstructure, with the particle size increasing as the nitrogen concentration is increased from 5 to 15 mol%, respectively. The pore size distribution of the samples is primarily from 2 to 33 nm. After 7 days of soaking in SBF, a large amount of blooming flower-like hydroxyapatite was deposited on the sample's surface with 15% of N_2, demonstrating excellent apatite-forming ability. It has been reported that incorporating nitrogen can stimulate cell proliferation during the early stages of incubation. It has been shown the 15% nitrogen can stimulate cell proliferation during the early stages of incubation. Additionally, the cytotoxicity was determined by measuring the optical density of hPDLCs incubated for 1, 3, and 7 days in an α-MEM medium containing various samples. None of the samples had an apparent inhibitory effect on the growth of hPDLCs at their extracted concentrations.

Letaïef et al. (Letaïef et al. 2014) compared HA layer formation using two templates (CTAB and triblock copolymer P123) to synthesize bioglass $92SiO_2$–6CaO–$2P_2O_5$. The sample synthesized with the CTAB exhibited a mesoporous structure. Using a cationic surfactant (CTAB) likely resulted in the absence of regular and periodic arrangement. Instead, the dense well-defined spherical mesoporous glass particles were obtained. The surface of the scaffold was completely covered in calcium phosphate crystallites. Using the triblock copolymer P123, on the other hand, led to the formation of an ordered mesoporous glass with a smooth morphology. Furthermore, increased pore volume, pore size, and specific area result in rapid ionic exchanges with the surrounding medium, contributing to the high bioactivity of the P123 samples. Indeed, after only 2 days of immersion in SBF, BG-P123 developed a thin HA layer on the surface. This apatite phase proliferated and crystallized after 15 days of immersing in SBF, demonstrating that the BG-P123 samples formed crystalline apatite at the fastest rate (Letaïef et al. 2014).

In another study, Lalzawmliana et al. (Lalzawmliana et al. 2019) investigated bioactivity by synthesizing MBG using a variety of different templates, including CTAB, polyethylene glycol (PEG), and pluronic P123. CTAB-MBG and

PEG-MBG demonstrated increased crystallinity, whereas P123-MBG revealed a slight reduction in the crystalline peak of $CaCO_3$ and an increase in the HA phase after 14 days in SBF solution. Moreover, the increased Ca-P layer formation in CTAB-MBG and PEG-MBG supported subsequent in vivo experiments to determine their bone regeneration efficacy combined with 50 µg of insulin-like growth factors (IGF-1) in a rabbit femur bone defect model, and bone samples were collected at 45 and 90 days. The results showed all MBGs had a high degree of new bone formation, i.e., CTAB-MBG (80.7 ± 2.9%), PEG-MBG (74.4 ± 2.4%), and P123-MBG (70.1 ± 1.9%) compared to MBG (66.9 ± 1.8%) (Lalzawmliana et al. 2019).

Diverse templates

Dong et al. (Dong et al. 2002) used zeolitic wood cells as the template for BG synthesizing. Firuzeh et al. (Firuzeh et al. 2021) used a templating agent of hexadecyltrimethylammonium p-toluenesulfonate (CTAT) to synthesize nanosphere bioglass with a 24-nm particle size, 9.73-nm pore diameter, and a high surface area (197 $m^2 g^{-1}$). An anion competition mechanism in which tosylate anions participate with silicate oligomers during particle formation could explain the enlargement of the mesopores (Firuzeh et al. 2021).

The pollen-templated bioglass particles had a dual macro-nanoporous structure. The 1-µm pores were inherited from the pollen grain template, whereas the sol–gel process's intrinsic mechanism induced the 9.5-nm pores. The specific surface area of templated bioglass was 111.4 $m^2 g^{-1}$, and the pore volume was 0.35 $cm^3 g^{-1}$ (Zheng et al. 2015).

Shoaib et al. (Shoaib et al. 2021) used F127 as the template to prepare spherical magnesium-doped mesoporous bioactive glass nanoparticles with a diameter of 65 ± 5 nm and a specific surface area (327 $m^2 g^{-1}$). The MTT assay revealed that the cytotoxicity of Mg-BG was negligible even at higher concentrations of 100 µg mL^{-1}.

A recent study used 15% cellulose nanofiber (CNF) as the sacrificial template to template the bioglass (Sarmast Sh et al. 2022). The result shows that by adding CNF, the particle size increased approximately 28% compared to pure BG. However, the porosity BG-templated was 45% more than pure BG, and the density was decreased by 32%. Cellulose nanofiber also affected the mechanical and swelling properties. The Young module was changed from 0.07 to 0.24 MPa. Pure BG had a high-water intake rate compared to BG-CNF, at 30% and 18% per day. The discharge rate of pure BG (was 3.3% per day), but BG-CNF absorbed a lower amount of water (18% per day).

Inverse opals are porous materials created by replicating silica opals in a three-dimensional order. They are composed of macropores connected by eight to twelve voids. Substances can migrate through the voids of macropores. Thus, it has been established that inverse opals are good templates for forming colloidal crystals and monodispersed microspheres (Yang et al. 2000). Furthermore, the inverse opal templates' restriction effect was confirmed to impact the final shape of microspheres significantly. Therefore, inverse opals may serve as useful templates to construct MBG microspheres containing high ion concentrations and surfactants, as their semi-closed pores can inhibit the migration of ions and molecules. As a result, their separation from the bioglass sol is hampered, and the surface effect influences their distribution (Ji et al. 2019). Ji et al. (Ji et al. 2019) used polystyrene film (OMP) and carbon film (OMC) to synthesize magnetic bioglass (by doping Fe^{3+}) for simulating the pore walls and templates at two different sintering temperatures (600 and 800 °C). They reported the OMP is a hydrophobic template, and the OMC is a hydrophilic template. The morphology characterization showed that by removing the template at a sintering temperature of 600 °C, OMP developed a microsphere structure (or-MBG). The or-MBG specific surface area was 474 $m^2 g^{-1}$. However, by increasing the sintering temperature to 800 °C, it was possible to obtain a core–shell structure with disordered mesopores (cs-MBG). However, the specific surface area of or-MBG was reduced to 127 $m^2 g^{-1}$. As indicated by the TEM and mapping images of the cs-MBG microspheres, Ca dispersed only in a core with a diameter of 181 nm, while Fe dispersed in a core with a diameter of 186 nm, as indicated by the TEM and mapping images of the cs-MBG microspheres. At 600 °C, MBG microspheres with open surface pores (op-MBG) more prominent than 10 nm were achieved using OMC as a template.

The MBG microspheres without open surface pores and a similar disordered mesoporous structure (dis-MBG) were synthesized at 800 °C. The op-MBG microspheres had a specific surface area of 211 $m^2 g^{-1}$, whereas the dis-MBG microspheres had only 47 $m^2 g^{-1}$. Although the iron concentration was the same, the magnetization saturation (M_s) values and magnetic properties of the samples were varied. M_s values for or-MBGs and op-MBGs were 0.117 and 0.143 emu g^{-1}, respectively. M_s values for cs-MBG and dis-MBG microspheres were approximately 0.091 and 0.173 emu g^{-1}, respectively. This could be because iron oxide particles formed at low temperatures were smaller than the magnetic field. Those formed at high temperatures, on the other hand, were larger due to agglomeration (Ji et al. 2019).

Bacterial cellulose (BC) has also been extensively investigated for use as a templating material in bone tissue engineering due to its naturally refined 3D nanofibrous network with a shape similar to natural collagen nanofibers (Luo et al. 2017). Generally, BC was used as a sacrificial template, and BC was burned out during the calcination step. The hydroxyl groups (–OH) on the surface of BC act as a catalyst to accelerate the hydrolysis and condensation reaction of

precursors (Luo et al. 2017a, b). Luo et al. (Luo et al. 2017a, b) used a BC nanofibrous scaffold as a template to fabricate a binary BG nanofibrous scaffold. The BC scaffold was first pre-calcified to absorb Ca^{2+} ions in a typical procedure. The pre-calcified BC scaffold was soaked in a TEOS and EtOH aqueous solution at room temperature for 6 h. The silica precursors were adsorbed to the BC nanofibers surface by ionic interaction between the hydroxyl (–OH) groups of the cellulose and free Ca^{2+} cations. The calcium ions could bond to silica colloid particles and form a calcium-silica layer on the BC surface. The final calcium silicate bioglass had nanofibers structure with a 16-nm diameter. A dense layer of HA appeared on the scaffold surface after only 1 day of immersion in 1.5 SBF. The larger surface area of the scaffold was due to high bioactivity (Luo et al. 2017a, b). Another research by Luo et al. (Luo et al. 2017a, b) synthesized a 58S bioglass scaffold with assisting of BC as a template. The scaffold revealed 75.1% porosity with a large surface area (127.4 $m^2\ g^{-1}$). The scaffold contained 39.4-nm diameter of mesopores and 60-µm diameter of macropores.

Xiao et al. (Xiao et al. 2019) synthesized the hallow mesoporous nanofibers using BC and pluronic P123 templates. The hydroxyl groups of promoting the hallow mesoporous nanofiber formation. The synthesized nanofibers had a 40-nm diameter, 8-nm wall thickness, and a 579.0 $m^2\ g^{-1}$specific surface area. The nanopore sizes of the wall of the scaffold were 3.9 nm- and 15.1-nm pores formed by neighboring tubes.

Wen et al. (Wen et al. 2018) used ultrasonic treatment to prepare a 3D nanofibrous BG scaffold using amino-modified bacterial cellulose as a template. Their results indicated that the amino groups on the BC template could effectively enhance the absorption of the deposited CaO and SiO_2 precursors. As a result, the BG scaffold exhibited a three-dimensional interconnected porous network structure composed of nanofibers with a diameter of approximately 20 nm. Furthermore, the scaffold was soaked in SBF for 1 to 7 days. The SEM result showed the morphology of the HA changed from a needle-like structure to a blooming flower-like structure, indicating rapid nucleation and growth of the HA crystallites as the immersed time increased.

Polymeric template

In 2010, Hong et al. introduced mesoporous bioglass (MBG) fibers. He developed MBG fibers by controlling the templating process (polyethylene oxide was used as the template) and the electrospinning conditions to enhance ultrathin MBG fibers with ~ 600-nm diameter, hollow cores, and mesoporous walls (Hong et al. 2010). It has been documented that the ideal range for the 3D fibrous structure is between 0.5 and 2 µm for complex tissue defects with great inter-fiber spaces to promote vascularization, cell penetration, and nutrient transportation throughout (Baino et al. 2016). Abad-Javier et al. (Abad-Javier et al. 2019) coupled sol–gel with spray-drying and used a polystyrene microsphere template to prepare the scaffold. They also functionalized the surface of the scaffold with collagen type I and vitamin D3 to increase its bioactivity. The result showed HA covered more than 70% of the scaffold surface.

Chitosan or PEG solution could be used as a liquid-based template by adding to the soil mixture. The result shows the diameter of BG has a range of 5–10 µm with 5–40-nm pore. This structure could support human marrow mesenchymal stem cells (hMSCs) attachment and proliferation. Liu et al. (W. Liu et al. 2012) developed a bioactive PEG/(SiO_2–CaO–P_2O_5) hybrid xerogel by hybridizing it with a SiO_2 component. As determined by characterization tests, the average pore diameter was 11.4 nm, with 7.2 $m^2\ g^{-1}$ of surface area. The bioactivity test established that adding PEG has no detrimental effect on the reactions between Si, Ca, and OH^-, CO_3^{2-} ions in the SBF solution. Additionally, the mechanical test revealed an increase in Young's modulus value to 430 MPa. Qian et al. used sugarcane as a template to produce a biomorphic 45S5 bioglass. In this method, the sugarcane was exposed to air before being sintered for 1 h at 1030 °C. Sugarcane's inherent microstructure was well converted into a 45S5 bioglass scaffold, with only a reduction in average pore size. In another study, polyethylene glycol (PEG 6000) was used as a soft template to produce a mesoporous bioglass with a composition of ($49SiO_2$–$20CaO$–$20Na_2O$–$7K_2O_4$–P_2O_5 mol%) (Shoaib et al. 2017). The morphology study showed that the spherical structure was usefully synthesized with 1 µm approximate size and 21-nm pore size with a 189.53 $m^2\ g^{-1}$ surface area. The cell cycle caused no tissue damage in the in vivo study (even at a concentration of 80 g mL^{-1}). Histopathological results revealed no discernible differences in the typical architecture of the control group and BG-treated skin tissues, even at a dose concentration of 40 mg kg^{-1} of body weight of the animals, demonstrating the safety of BG (Shoaib et al. 2017).

It has been reported that hollow nano-spherical bioglasses were synthesized using the polyacrylic acid (PAA) template. Following air combustion, PAA was incorporated to form the core, whereas the inorganic shell was constructed using a precursor. As a result, they contained various (TEOS)/PAA concentrations in a glass network. In comparison, 0.2 g of the template PAA was maintained as the constant value (Wang & Chen 2017). The samples were labeled as HBG1, HBG2, HBG3, and HBG4 with 0.9, 1.8, 2.7, and 3.6 g of TEOS content. The results showed that shell thickness and particle size were raised by increasing TEOS concentration. However, a reduction in pore volume and specific surface area was obtained. The particle sizes for HBG1, HBG2, HBG3, and HBG4 nanospheres were 81.0 ± 15.6,

92.0 ± 14.7, 109.9 ± 21.3, and 133.3 ± 25.6 nm, respectively. The relatively high specific area of the HBG1 (50.16 m^2 g^{-1}) compared to other similar structures was due to the thin shell thickness. Additionally, the total pore volume of the obtained samples reduced from 0.129 to 0.072 cm^3 g^{-1} at 0.99 of the relative pressure (Liu et al. 2017).

Ali et al. (Ali et al. 2023) conducted a study to investigate the impact of irisin-loaded bioglass on pre-osteoblast behavior and regenerative potential. In their experimental design, they used a 70% polymethyl methacrylate (PMMA) and 150 ng/ml irisin as a sacrificial template. The controlled release of irisin was achieved by adding PVA as a binder. The bioglass, characterized by an 84.3% porosity, exhibited pores ranging in size from 100 to 300 µm. The results of the study relieved the influence of irisin's controlled release on osteogenic differentiation and calcium deposition in vitro. The in vivo findings demonstrated that the PVA-irisin-loaded bioglass significantly promoted the development of new bone in the defect areas. This was accompanied by the expression of osteogenic markers, such as ALP, Runx-2, and OPN, as well as the formation of structural proteins like Col-1 in a rat model.

A summary of templating roles is described in Table 5.

Discussion

The synthesis of bioglasses through various techniques has been extensively explored in recent years, with each method exhibiting unique advantages and drawbacks. The acid-/base-catalyzed sol–gel method using inorganic acids like nitric acid, sulfuric acid, and hydrochloric acid as catalysts results in the formation of small linear polymeric entities due to cross-linking of silanol/silanol or silanol/ethoxy groups. However, this approach often leads to weak structures tending to crumble upon drying, limiting their practical applications (Albert et al. 2017; Brinker and Scherer 2013; Zheng & Boccaccini 2017).

Microemulsion-based sol–gel synthesis offers improved homogeneity by preventing nanoparticle aggregation, yet excess surfactants and oil phase residues must be meticulously removed to avoid detrimental effects on the final product (Deshmukh et al. 2020; Zheng & Boccaccini 2017).

Modified sol–gel synthesis methods, such as ethanol washing, citric acid templating, colloidal techniques, and fast-drying methods, provide avenues for controlling the microstructure and properties of bioglasses (Ben-Arfa et al. 2018, 2020; Lopes et al. 2019; Mukundan et al. 2013; Spirandeli et al. 2020). Furthermore, the combination of sol–gel and electrospinning techniques facilitated the production of mesoporous bioglass fibers, creating intricate three-dimensional structures that support cell attachment and proliferation (Abad-Javier et al. 2019; Hong et al. 2010).

One of the key findings in this study is the significant influence of various templates on the structure and properties of bioglasses in sol–gel technique. The use of zeolitic wood cells, cellulose nanofibers, and bacterial cellulose templates led to the creation of bioglass scaffolds with enhanced porosity and specific surface area (Dong et al. 2002; Wen et al. 2018; Luo et al. 2017a, b). Templated sol–gel scaffolds with templates like hexadecyltrimethylammonium bromide (CTAB) and pluronic P123 demonstrated the formation of ordered mesoporous structures (Ji et al. 2019; Letaïef et al. 2014). Additionally, incorporating nitrogen into bioglasses using CTAB templates resulted in nanospheres with varying pore sizes and improved cell proliferation, indicating the potential of nitrogen-doped bioglasses for tissue engineering applications (Wen et al. 2022). Integrating polymeric templates, such as chitosan and polyethylene glycol, allowed for the fabrication of hybrid xerogels with favorable pore diameters and surface areas, enhancing the bioactivity of the resulting bioglasses (Liu et al. 2012).

The template selection in the sol–gel technique has a significant impact on tailoring the microstructure and properties of bioglasses. The various templating techniques explored in recent years offer valuable insights into the customization of bioglass structures for designing bone scaffolds.

Conclusion

Biological and biomedical applications of sol–gel silica glass have experienced significant growth in recent decades due to its ease of use and versatile control over the properties and morphology of silicate bioglass. The sol–gel technique offers various synthesis strategies that enable tailored manipulation of bioglass characteristics. Acid-/base-catalyzed synthesis facilitates rapid hydrolysis reactions using strong inorganic acids as catalysts, while base catalysis promotes cross-linking and the formation of complex polymer structures. Microemulsion-based synthesis ensures homogeneous compositions and allows for precise particle size and shape adjustment. Modified sol–gel synthesis strategies involving alternative precursors and catalysts have been developed to enhance bioactivity and enable microstructure control. Templated sol–gel scaffolds utilize diverse templates to create hierarchical pore architectures, allowing further customization of the bioglass's morphology and structure. Combining the sol–gel technique with different synthesis strategies offers significant potential for tailoring the properties of bioglass materials, including pore structure, surface area, bioactivity, and mechanical strength. Here, the key findings and advantages of different templating methods in the context of silica bioglass sol–gel synthesis have been summarized.

Table 5 Template roles in silica glass morphology

Template	*Bioglass*	*Method*	*Shape*	*Pore diameter (nm)*	*Surface area ($m^2\ g^{-1}$)*	*Pore volume ($cm^3\ g^{-1}$)*	*Reference*
Amino-modified bacterial cellulose	SiO_2–CaO	Ultrasonic treatment	Fiber	20	144.60	0.21	(Wen et al. 2018)
Bacterial cellulose	SiO_2–CaO	Freeze-dried	Fiber	25–36	240.9	0.331	(Luo et al. 2017a, b)
	58S	Sacrificial Template	Fiber	39.4	127.4	0.242	(Luo et al. 2017a, b)
Bacterial cellulose/pluronic P123	SiO_2–CaO–P_2O_5	Freeze-dried and sacrificial template	Hallow fiber	3.9	579		(Xiao et al. 2019)
Cellulose nanofiber	45S5	Sacrificial template	Fiber	91.55	4.864	0.223	(Sarmast Sh et al. 2022)
Chitosan	$60SiO_2$–36CaO–$4P_2O_5$	Surfactant	Microspheres	5–10 µm	1.8	0.02	(Lei et al. 2012)
Hexadecyltrimethylammonium bromide (CTAB)	SiO_2–CaO–P_2O_5	Surfactant solution and freeze-dried	Hollow mesoporous	7	321	0.85	(Xie et al. 2020)
	SiO_2–CaO–P_2O_5	Surfactant solution	Spherical	3.6	473.2	0.27	(Anand et al. 2018)
	$60SiO_2$–30.8CaO–$9.2P_2O_5$	Surfactant solution	Spherical	8–11	225–271	0.62–0.67	(Wen et al. 2022)
CTAB/copolymer P123	$92SiO_2$–6CaO–$2P_2O_5$	Surfactant solution	Spherical	5.7	376.7	0.66	(Letaïef et al. 2014)
Hexadecyltrimethylammonium p-toluenesulfonate (CTAT)	SiO_2–CaO–P_2O_5	surfactant solution	Spherical	9.73	197	0.48	(Firuzeh et al. 2021)
Methyl cellulose		Sacrificial template	Spherical		472		(Gupta & Santhiya 2017)
Pluronic F127	$51SiO_2$–18CaO–$20Na_2O$–$4P_2O_5$–7MgO	Surfactant solution	Spherical	65	327		(Shoaib et al. 2021)
Pluronic P123	SiO_2–CaO–P_2O_5	Surfactant solution	Spherical	8.9	169.3	0.285	(Anand et al. 2018)
Pluronic P123/pluronic F127/polyurethane	MBG	Surfactant solution		3.3–19.6	375.1–1105.8	0.68–1.33	(Xia et al. 2022)
Pollen	$70SiO_2$–30CaO	Sacrificial template	Dual macro-nanoporous	1 µm and 9.5 nm	111.4	0.35	(Zheng et al. 2015)
Poly acrylic acid (PAA)	SiO_2–CaO–P_2O_5	Sacrificial template	Hollow spherical	81.0–133.3	33.89–50.16	0.129–0.072	(Liu et al. 2017)
Poly amidoamine (PAMAM)	45S5	Surfactant solution	Polygonal	0.5–2	472		(Gupta et al. 2015)
Polyethylene glycol (PEG)	SiO_2–CaO–P_2O_5	Surfactant solution	Spherical	11.4	7.2	0.003	(Liu et al. 2012)
	SiO_2–CaO–P_2O_5	Surfactant solution	Cauliflower	15.6	52.2	0.087	(Anand et al. 2018)
	$49SiO_2$–20CaO–$20Na_2O$–$7K_2O_4$–P_2O_5	Surfactant solution	Spherical	21	189.53		(Shoaib et al. 2017)

Table 5 (continued)

Template	*Bioglass*	*Method*	*Shape*	*Pore diameter (nm)*	*Surface area ($m^2\ g^{-1}$)*	*Pore volume ($cm^3\ g^{-1}$)*	*Reference*
Polymethyl methacrylate (PMMA)	45S5	Sacrificial template		100–300 µm			(Ali et al. 2023)
Polystyrene/ carbon film	MBG	Surfactant solution and sacrificial template	Spherical	181–186	127–474		(Ji et al. 2019)
Rice husk	45S5	Sacrificial template		25–75 µm			(Wu et al. 2009)
Sugarcane	45S5	Sacrificial template	Biomorphic	5–10 µm			
Zeolitic wood cells		Sacrificial template	Hollow Fiber	55–165	315	0.12	(Dong et al. 2002)

Surfactant-based templating

Surfactant templating methods, such as microemulsion-based synthesis and CTAB-assisted synthesis, have enabled the creation of mesoporous bioactive glasses with well-defined pore structures.

Surfactants play a crucial role in stabilizing microemulsion droplets and controlling the size and shape of pores, leading to enhanced surface area and improved bioactivity.

Polymeric templating

Polymeric templates, including PEG and chitosan, have been used to fabricate bioactive glass scaffolds with interconnected pores and suitable mechanical properties.

Polymer-based templates offer flexibility in controlling the scaffold's morphology and pore size, promoting cell attachment, proliferation, and tissue regeneration.

Natural templates

Natural templates, such as sugarcane and bacterial cellulose, provide unique hierarchical structures that can be replicated in bioactive glasses.

The inherent microstructure of natural templates can be preserved, resulting in biomorphic bioactive glasses with tailored properties for specific applications.

Hybrid templating approaches

Hybrid approaches, combining different templating methods or incorporating multiple template materials, allow for precisely engineering complex structures and functionalities.

By integrating surfactant-assisted and polymeric templating techniques, researchers can achieve synergistic effects, leading to superior bioactive glass materials.

Templating techniques significantly enhance the bioactivity of bioactive glasses by increasing surface area, pore volume, and pore interconnectivity. The tailored structures created through templating methods promote improved ion release, mineralization, and cell-material interactions, making them highly biocompatible for various biomedical applications. Continued research in templating techniques should focus on optimizing parameters, such as template concentration, processing conditions, and choice of template material, to further enhance the properties of bioactive glasses. Exploration of innovative natural templates and developing hybrid templating strategies hold promising avenues for creating bioactive glasses with advanced functionalities tailored for specific clinical needs. Addressing challenges related to scalability, cost-effectiveness, and regulatory approvals will be essential for translating templated bioactive glasses from research laboratories to practical orthopedic medical applications.

Acknowledgements The authors sincerely thank Associate Professor Farideh Zafari Zangeneh from the Reproductive Health Research Center, Tehran University of Medical Sciences, for kindly performing professional editing in this paper.

Funding Open Access funding provided by the IReL Consortium The work was funded by Universiti Putra Malaysia under Geran Putra Inisiatif Siswazah (9669500).

Declarations

Conflict of interest Dayang Radiah Awang Biak reports financial support was provided by Universiti Putra Malaysia under Geran Putra Inisiatif Siswazah (9669500). All other authors declare no competing interests.

References

Abad-Javier ME, Cajero-Juárez M, Nuñez-Anita RE, Contreras-García ME. Effect of collagen type I and vitamin D3 functionalization of biomimetic bioglass scaffolds on hydroxyapatite condensation. J Eur Ceram Soc. 2019;39(12):3505–12. https://doi.org/10.1016/j.jeurceramsoc.2019.02.050.

Albert K, Huang XC, Hsu HY. Bio-templated silica composites for next-generation biomedical applications. Adv Colloid Interface Sci. 2017;249:272–89. https://doi.org/10.1016/j.cis.2017.04.011. (**Elsevier B.V.**).

Ali M, Farwa U, Park SS, Kim YS, Lee BT. Physico-biological and in vivo evaluation of irisin loaded 45S5 porous bioglass granules for bone regeneration. Biomater Adv. 2023;147:213326. https://doi.org/10.1016/J.BIOADV.2023.213326.

Anand A, Kundu B, Balla VK, Nandi SK. Synthesis and physicochemical characterization of different mesoporous bioactive glass nanopowders: in-vitro SBF activity and cytotoxicity. Trans Indian Ceram Soc. 2018;77(2):106–17. https://doi.org/10.1080/0371750X.2018.1465357.

Arcos D, Vallet-Regí M. Sol-gel silica-based biomaterials and bone tissue regeneration. Acta Biomater. 2010;6(8):2874–88. https://doi.org/10.1016/j.actbio.2010.02.012.

Baino F, Fiorilli S, Vitale-Brovarone C. Bioactive glass-based materials with hierarchical porosity for medical applications: review of recent advances. Acta Biomater. 2016;42:18–32. https://doi.org/10.1016/j.actbio.2016.06.033.

Baino F. Bioactive glasses and glass-ceramics. In: Encyclopedia of Materials: Technical Ceramics and Glasses. 2021. (pp. 614–623). Elsevier. https://doi.org/10.1016/B978-0-12-803581-8.12088-0.

Bellucci D, Anesi A, Salvatori R, Chiarini L, Cannillo V. A comparative in vivo evaluation of bioactive glasses and bioactive glass-based composites for bone tissue repair. Mater Sci Eng C. 2017;79:286–95. https://doi.org/10.1016/j.msec.2017.05.062.

Ben-Arfa BAE, Salvado IMM, Ferreira JMF, Pullar RC. Enhanced bioactivity of a rapidly-dried sol-gel derived quaternary bioglass. Mater Sci Eng C. 2018;91(October 2017):36–43. https://doi.org/10.1016/j.msec.2018.05.016.

Ben-Arfa BAE, Palamá IE, Miranda Salvado IM, Ferreira JMF, Pullar RC. The role of calcium (source & content) on the in vitro behaviour of sol–gel quaternary glass series. Ceram Int. 2020;46(1):1065–75. https://doi.org/10.1016/J.CERAMINT.2019.09.073.

Bokov D, Turki Jalil A, Chupradit S, Suksatan W, Javed Ansari M, Shewael IH, Valiev GH, Kianfar E. Nanomaterial by sol-gel method: synthesis and application. Adv Mater Sci Eng. 2021;2021. https://doi.org/10.1155/2021/5102014. (**Hindawi Limited**).

Brauer DS. Bioactive glasses - structure and properties. Angew Chem - Int Ed. 2015;54(14):4160–81. https://doi.org/10.1002/anie.201405310.

Brinker CJ, Scherer GW. Sol-gel science: the physics and chemistry of sol-gel processing. Academic Press INC. 2013. https://books.google.com.my/books?hl=en&lr=&id=CND1BAAAQBAJ&oi=fnd&pg=PP1&ots=afxJI3YhcG&sig=VIACwMhRAiNHicGvceHCb2jGL6o&redir_esc=y#v=onepage&q&f=false.

Chen QZ, Thouas GA. Fabrication and characterization of sol-gel derived 45S5 Bioglass®-ceramic scaffolds. Acta Biomater. 2011;7(10):3616–26. https://doi.org/10.1016/j.actbio.2011.06.005.

Crovace MC, Souza MT, Chinaglia CR, Peitl O, Zanotto ED. Biosilicate?? - A multipurpose, highly bioactive glass-ceramic. in vitro, in vivo and clinical trials. J Non-Cryst Solids. 2016;432:90–110. https://doi.org/10.1016/j.jnoncrysol.2015.03.022.

Deepthi S, Venkatesan J, Kim S-K, Bumgardner JD, Jayakumar R. An overview of chitin or chitosan/nano ceramic composite scaffolds for bone tissue engineering. Int J Biol Macromol. 2016;93:1338–53. https://doi.org/10.1016/j.ijbiomac.2016.03.041.

Deshmukh K, Kovářík T, Křenek T, Docheva D, Stich T, Pola J. Recent advances and future perspectives of sol-gel derived porous bioactive glasses: a review. RSC Adv. 2020;10(56):33782–835. https://doi.org/10.1039/d0ra04287k. (**Royal Society of Chemistry**).

Dong A, Wang Y, Tang Y, Ren N, Zhang Y, Yue Y, Gao Z. Zeolitic tissue through wood cell templating. Adv Mater. 2002;14(12):926–9. https://doi.org/10.1002/1521-4095(20020618)14:12%3c926::AID-ADMA926%3e3.0.CO;2-1.

Dziadek M, Stodolak-Zych E, Cholewa-Kowalska K. Biodegradable ceramic-polymer composites for biomedical applications: a review. Mater Sci Eng C. 2017;71:1175–91. https://doi.org/10.1016/j.msec.2016.10.014.

El-Rashidy AA, Roether JA, Harhaus L, Kneser U, Boccaccini AR. Regenerating bone with bioactive glass scaffolds: a review of in vivo studies in bone defect models. Acta Biomater. 2017;62:1–28. https://doi.org/10.1016/j.actbio.2017.08.030.

Fantecelle FB, dos Santos DMM, Barrioni BR, Pereira MM, Alcamand HA, Lapér ML, Houmard M, Nunes EHM. Structural, mechanical, and in vitro characterization of freeze-cast scaffolds prepared using a sol-gel-derived bioactive glass from the SiO2–CaO–Na2O–P2O5–K2O–MgO system. Ceram Int. 2023;49(2):2183–93. https://doi.org/10.1016/j.ceramint.2022.09.185.

Faure J, Drevet R, Lemelle A, Ben Jaber N, Tara A, El Btaouri H, Benhayoune H. A new sol-gel synthesis of 45S5 bioactive glass using an organic acid as catalyst. Mater Sci Eng C. 2015;47:407–12. https://doi.org/10.1016/j.msec.2014.11.045.

Firuzeh M, Labbaf S, Sabouri Z. A facile synthesis of mono-dispersed, spherical and mesoporous bioactive glass nanoparticles for biomedical applications. J Non-Cryst Solids. 2021;554. https://doi.org/10.1016/j.jnoncrysol.2020.120598.

Fu Q, Saiz E, Rahaman MN, Tomsia AP. Bioactive glass scaffolds for bone tissue engineering: state of the art and future perspectives. Mater Sci Eng C Mater Biol Appl. 2012;31(7):1245–56. https://doi.org/10.1016/j.msec.2011.04.022.Bioactive.

Ge YW, Lu JW, Sun ZY, Liu ZQ, Zhou J, Ke QF, Mao YQ, Guo YP, Zhu ZA. Ursolic acid loaded-mesoporous bioglass/chitosan porous scaffolds as drug delivery system for bone regeneration. Nanomedicine: Nanotechnol Biol Med. 2019;18:336–46. https://doi.org/10.1016/j.nano.2018.10.010.

Guo W, Zhao F, Wang Y, Tang J, Chen X. Characterization of the mechanical behaviors and bioactivity of tetrapod ZnO whiskers reinforced bioactive glass/gelatin composite scaffolds. J Mech Behav Biomed Mater. 2017;68(November 2016):8–15. https://doi.org/10.1016/j.jmbbm.2017.01.032.

Gupta N, Santhiya D. Role of cellulose functionality in bio-inspired synthesis of nano bioactive glass. Mater Sci Eng C. 2017;75:1206–13. https://doi.org/10.1016/j.msec.2017.03.026.

Gupta N, Santhiya D, Aditya A, Badra K. Dendrimer templated bioactive glass-ceramic nanovehicle for gene delivery applications.

RSC Adv. 2015;5(70):56794–807. https://doi.org/10.1039/C5RA04441C.

Hong Y, Chen X, Jing X, Fan H, Guo B, Gu Z, Zhang X. Preparation, bioactivity, and drug release of hierarchical nanoporous bioactive glass ultrathin fibers. Adv Mater. 2010;22(6):754–8. https://doi.org/10.1002/adma.200901656.

Hu Q, Li Y, Zhao N, Ning C, Chen X. Facile synthesis of hollow mesoporous bioactive glass sub-micron spheres with a tunable cavity size. Mater Lett. 2014;134:130–3. https://doi.org/10.1016/j.matlet.2014.07.041.

Huang K, Cai S, Xu G, Ye X, Dou Y, Ren M, Wang X. Preparation and characterization of mesoporous 45S5 bioactive glass – ceramic coatings on magnesium alloy for corrosion protection. J Alloy Compd. 2013;580:290–7. https://doi.org/10.1016/j.jallcom.2013.05.103.

Ji L, Gong M, Xu T, Gu J, Jiang X, Liang T, Chen Y, Liu Q. Engineering the structure of mesoporous bioactive glass microspheres by the surface effect of inverse opal templates and temperature. Small. 2019;15(52). https://doi.org/10.1002/smll.201905451.

Jones JR. Acta Biomaterialia Editor's Comment on : Review of bioactive glass : from Hench to hybrids. 2015;23:2015. https://doi.org/10.1016/j.actbio.2015.07.005.

Kaur G, Pandey OP, Singh K, Homa D, Scott B, Pickrell G. A review of bioactive glasses: their structure, properties, fabrication and apatite formation. J Biomed Mater Res - Part A. 2014;102(1):254–74. https://doi.org/10.1002/jbm.a.34690.

Kaur G, Pickrell G, Sriranganathan N, Kumar V, Homa D. Review and the state of the art: Sol–gel and melt quenched bioactive glasses for tissue engineering. J Biomed Mater Res - Part B Appl Biomater. 2016;104(6):1248–75. https://doi.org/10.1002/jbm.b.33443.

Kokubo T, Takadama H. How useful is SBF in predicting in vivo bone bioactivity? Biomaterials. 2006;27(15):2907–15. https://doi.org/10.1016/j.biomaterials.2006.01.017.

Lalzawmliana V, Anand A, Kumar V, Das P, Devi KB, Mukherjee J, Maji AK, Kundu B, Roy M, Nandi SK. Potential of growth factor incorporated mesoporous bioactive glass for in vivo bone regeneration. J Mech Behav Biomed Mater. 2019;91:182–92. https://doi.org/10.1016/j.jmbbm.2018.12.012.

Lei B, Shin KH, Moon YW, Noh DY, Koh YH, Jin Y, Kim HE. Synthesis and bioactivity of sol-gel derived porous, bioactive glass microspheres using chitosan as novel biomolecular template. J Am Ceram Soc. 2012;95(1):30–3. https://doi.org/10.1111/j.1551-2916.2011.04918.x.

Lei Q, Guo J, Noureddine A, Wang A, Wuttke S, Brinker CJ, Zhu W. Sol–gel-based advanced porous silica materials for biomedical applications. Adv Funct Mater. 2020;30:41. https://doi.org/10.1002/adfm.201909539. (**Wiley-VCH Verlag**).

Letaïef N, Lucas-Girot A, Oudadesse H, Dorbez-Sridi R, Boullay P. Investigation of the surfactant type effect on characteristics and bioactivity of new mesoporous bioactive glass in the ternary system SiO2–CaO–P2O5: Structural, textural and reactivity studies. Microporous Mesoporous Mater. 2014;195:102–11. https://doi.org/10.1016/J.MICROMESO.2014.03.035.

Li Y, Chen X, Ning C, Yuan B, Hu Q. Facile synthesis of mesoporous bioactive glasses with controlled shapes. Mater Lett. 2015;161:605–8. https://doi.org/10.1016/j.matlet.2015.09.057.

Li R. Sol-gel processing of bioactive glass powders : Li, Rounan, 1945- : Free Download & Streaming : Internet Archive [University of Florida]. 1991. https://doi.org/10.1002/jab.770020403.

Liang Q, Hu Q, Miao G, Yuan B, Chen X. A facile synthesis of novel mesoporous bioactive glass nanoparticles with various morphologies and tunable mesostructure by sacrificial liquid template method. Mater Lett. 2015;148:45–9. https://doi.org/10.1016/J.MATLET.2015.01.122.

Liu W, Wu X, Zhan H, Yan F. Synthesis of bioactive poly(ethylene glycol)/SiO2-CaO-P2O5 hybrids for bone regeneration. Mater Sci Eng C. 2012;32(4):707–11. https://doi.org/10.1016/J.MSEC.2012.01.012.

Liu T, Li Z, Ding X, Zhang L, Zi Y. Facile synthesis of hollow bioactive glass nanospheres with tunable size. Mater Lett. 2017;190:99–102. https://doi.org/10.1016/j.matlet.2016.12.129.

Lopes JH, Bueno OMVM, Mazali IO, Bertran CA. Investigation of citric acid-assisted sol-gel synthesis coupled to the self-propagating combustion method for preparing bioactive glass with high structural homogeneity. Mater Sci Eng, C. 2019;97:669–78. https://doi.org/10.1016/J.MSEC.2018.12.022.

Luo H, Zhang Y, Wang Z, Yang Z, Tu J, Liu Z, Yao F, Xiong G, Wan Y. Constructing three-dimensional nanofibrous bioglass/gelatin nanocomposite scaffold for enhanced mechanical and biological performance. Chem Eng J. 2017;326:210–21. https://doi.org/10.1016/J.CEJ.2017.05.115.

Luo H, Li W, Ao H, Li G, Tu J, Xiong G, Zhu Y, Wan Y. Preparation, structural characterization, and in vitro cell studies of three-dimensional SiO 2 – CaO binary glass scaffolds built of ultra-small nano fi bers. Mater Sci Eng C. 2017a;76:94–101. https://doi.org/10.1016/j.msec.2017.02.134.

Luo H, Zhang Y, Li G, Tu J, Yang Z, Xiong G, Wang Z, Huang Y, Wan Y. Sacrificial template method for the synthesis of three-dimensional nanofibrous 58S bioglass scaffold and its in vitro bioactivity and cell responses. J Biomater Appl. 2017b;32(2):265–75. https://doi.org/10.1177/0885328217715784.

Modan EM, Plăiașu AG. Advantages and disadvantages of chemical methods in the elaboration of nanomaterials. Ann "Dunarea de Jos" Univ Galati Fascicle IX Metall Mater Sci. 2020;43(1)53–60. https://doi.org/10.35219/mms.2020.1.08.

Mukundan LM, Nirmal R, Vaikkath D, Nair PD. A new synthesis route to high surface area sol gel bioactive glass through alcohol washing: a preliminary study. Biomatter. 2013;3(2):1–10. https://doi.org/10.4161/biom.24288.

Naleway SE, Porter MM, McKittrick J, Meyers MA. Structural design elements in biological materials: application to bioinspiration. Adv Mater. 2015;27(37):5455–76. https://doi.org/10.1002/adma.201502403. (**Wiley-VCH Verlag**).

Nawaz Q, de Pablos-Martín A, Contreras Jaimes AT, Scheffler F, Wagner T, Brauer DS, Boccaccini AR. Comparison of microstructure, sintering behavior, and biological response of sol-gel and melt-derived 13–93 bioactive glass scaffolds. Open Ceram. 2023;15. https://doi.org/10.1016/j.oceram.2023.100407.

Owens GJ, Singh RK, Foroutan F, Alqaysi M, Han C-M, Mahapatra C, Kim H-W, Knowles JC. Sol–gel based materials for biomedical applications. Prog Mater Sci. 2016;77:1–79. https://doi.org/10.1016/J.PMATSCI.2015.12.001.

Peltola T, Jokinen M, Rahiala H, Lev?nen E, Rosenholm JB, Kangasniemi I, Yli-Urpo A. Calcium phosphate formation on porous sol-gel-derived SiO_2 and $CaO-P_2O_5-SiO_2$ substrates in vitro. J Biomed Mater Res. 1999;44(1). https://doi.org/10.1002/(SICI)1097-4636(199901)44:1<12::AID-JBM2>3.0.CO;2-E.

Qian J, Kang Y, Wei Z, Zhang W. Fabrication and characterization of biomorphic 45S5 bioglass scaffold from sugarcane. Mater Sci Eng C. 2009;29(4):1361–4. https://doi.org/10.1016/j.msec.2008.11.004.

Sarmast Sh M, George S, Dayang Radiah AB, Hoey D, Abdullah N, Kamarudin S. Synthesis of bioactive glass using cellulose nano fibre template. J Mech Behav Biomed Mater. 2022;130:105174. https://doi.org/10.1016/j.jmbbm.2022.105174.

Shoaib M, Bahadur A, Iqbal S, AL-Anazy MM, Laref A, Tahir MA, Channar PA, Noreen S, Yasir M, Iqbal A, Ali KW. Magnesium doped mesoporous bioactive glass nanoparticles: a promising material for apatite formation and mitomycin c delivery to the

MG-63 cancer cells. J Alloys Compd. 2021;866. https://doi.org/10.1016/j.jallcom.2021.159013.

Shoaib M, Saeed A, Akhtar J, Saif M, Rahman U, Ullah A, Jurkschat K, Moazzam M. Potassium-doped mesoporous bioactive glass : Synthesis , characterization and evaluation of biomedical properties. 2017;75:836–844. https://doi.org/10.1016/j.msec.2017.02.090

Siqueira RL, Peitl O, Zanotto ED. Gel-derived SiO2–CaO–Na2O–P2O5 bioactive powders: Synthesis and in vitro bioactivity. Mater Sci Eng C. 2011;31(5):983–91. https://doi.org/10.1016/j.msec.2011.02.018.

Spirandeli BR, Campos TMB, Ribas RG, Thim GP, de Sousa Trichês E. Evaluation of colloidal and polymeric routes in sol-gel synthesis of a bioactive glass-ceramic derived from 45S5 bioglass. Ceram Int. 2020;46(12):20264–71. https://doi.org/10.1016/J.CERAMINT.2020.05.108.

Venkatraman SK, Swamiappan S. Review on calcium- and magnesium-based silicates for bone tissue engineering applications. J Biomed Mater Res - Part A. 2020;108(7):1546–62. https://doi.org/10.1002/jbm.a.36925.

Wan YZ, Luo H, He F, Liang H, Huang Y, Li XL. Mechanical, moisture absorption, and biodegradation behaviours of bacterial cellulose fibre-reinforced starch biocomposites. Compos Sci Technol. 2009;69(7–8):1212–7. https://doi.org/10.1016/j.compscitech.2009.02.024.

Wang Y, Chen X. Facile synthesis of hollow mesoporous bioactive glasses with tunable shell thickness and good monodispersity by micro-emulsion method. Mater Lett. 2017;189:325–8. https://doi.org/10.1016/J.MATLET.2016.12.004.

Wen C, Hong Y, Wu J, Luo L, Qiu Y, Ye J. The facile synthesis and bioactivity of a 3D nanofibrous bioglass scaffold using an amino-modified bacterial cellulose template. RSC Adv. 2018;8(26):14561–9. https://doi.org/10.1039/C8RA00352A.

Wen C, Qian J, Luo L, Zeng J, Sa B, Zhan X, Wang J, Sheng L, Zheng Y. Effect of nitrogen on the structure evolution and biological properties of mesoporous bioactive glass nanospheres: Experiments and simulations. J Non-Crystalline Solids. 2022;578. https://doi.org/10.1016/j.jnoncrysol.2021.121329.

Woignier T, Scherer GW, Alaoui A. Stress in aerogel during depressurization of autoclave: II. Silica gels. J Sol-Gel Sci Technol. 1994;3(2):141–50. https://doi.org/10.1007/BF00486720.

Wu S-C, Hsu H-C, Hsiao S-H, Ho W-F. Preparation of porous 45S5 Bioglass®-derived glass–ceramic scaffolds by using rice husk as a porogen additive. J Mater Sci - Mater Med. 2009;20(6):1229–36. https://doi.org/10.1007/s10856-009-3690-8.

Xia W, Chang J. Preparation and characterization of nano-bioactive-glasses (NBG) by a quick alkali-mediated sol–gel method. Mater Lett. 2007;61(14–15):3251–3. https://doi.org/10.1016/J.MATLET.2006.11.048.

Xia D, Wang Y, Wu R, Zheng Q, Zhang G, Xu S, Zhou P. The effect of pore size on cell behavior in mesoporous bioglass scaffolds for bone regeneration. Appl Mater Today. 2022;29:101607. https://doi.org/10.1016/J.APMT.2022.101607.

Xiao J, Wan Y, Yao F, Huang Y, Zhu Y, Yang Z, Luo H. Constructing 3D scaffold with 40-nm-diameter hollow mesoporous bioactive glass nanofibers. Mater Lett. 2019;248:201–3. https://doi.org/10.1016/J.MATLET.2019.04.041.

Xie W, Chen X, Li Y, Miao G, Wang G, Tian T, Zeng L, Chen X. Facile synthesis and in vitro bioactivity of radial mesoporous bioactive glass with high phosphorus and calcium content. Adv Powder Technol. 2020;31(8):3307–17. https://doi.org/10.1016/j.apt.2020.06.021.

Yang SM, Coombs N, Ozin GA. Micromolding in Inverted Polymer Opals (MIPO): Synthesis of Hexagonal Mesoporous Silica Opals. Adv Mater. 2000;12(24):1940–4. https://doi.org/10.1002/1521-4095(200012)12:24%3c1940::AID-ADMA1940%3e3.0.CO;2-D.

Zheng K, Boccaccini AR. Sol-gel processing of bioactive glass nanoparticles: A review. Adv Colloid Interface Sci. 2017;1–11. https://doi.org/10.1016/j.cis.2017.03.008.

Zheng K, Bortuzzo JA, Liu Y, Li W, Pischetsrieder M, Roether J, Lu M, Boccaccini AR. Bio-templated bioactive glass particles with hierarchical macro–nano porous structure and drug delivery capability. Colloids Surf B. 2015;135:825–32. https://doi.org/10.1016/j.colsurfb.2015.03.038.